Published in final edited form as:
Bioconjug Chem. 2012 August 15; 23(8): 1548–1556. doi:10.1021/bc300009t.

Synthesis and evaluation of a peptide targeted small molecular Gd-DOTA monoamide conjugate for MR molecular imaging of prostate cancer

Xueming Wu[1], **Susan M. Burden-Gulley**[2], **Guan-Ping Yu**[1], **Mingqian Tan**[1], **Daniel Lindner**[3], **Susann M. Brady-Kalnay**[2], and **Zheng-Rong Lu**[1,†]

[1]Department of Biomedical Engineering, Case Western Reserve University, Cleveland, Ohio 44106, USA

[2]Department of Molecular Biology and Microbiology, School of Medicine, Case Western Reserve University, Cleveland, Ohio, USA

[3]Dept. of Translational Hematology & Oncology Research, Cleveland Clinic, Cleveland, Ohio 44195, USA

Abstract

Tumor extracellular matrix has an abundance of cancer related proteins that can be used as biomarkers for cancer molecular imaging. Innovative design and development of safe and effective targeted contrast agents to these biomarkers would allow effective MR cancer molecular imaging with high spatial resolution. In this study, we synthesized a low molecular weight CLT1 peptide targeted Gd(III) chelate CLT1-dL-$(Gd\text{-}DOTA)_4$ specific to clotted plasma proteins in tumor stroma for cancer MR molecular imaging. CLT1-dL-$(Gd\text{-}DOTA)_4$ was synthesized by conjugating four Gd-DOTA monoamide chelates to a CLT1 peptide via generation 1 lysine dendrimer. The T_1 relaxivity of CLT1-dL-$(Gd\text{-}DOTA)_4$ was 40.4 $mM^{-1}s^{-1}$ per molecule (10.1 $mM^{-1}s^{-1}$ per Gd) at 37 °C and 1.5 T. Fluorescence imaging showed high binding specificity of CLT1 to orthotopic PC3 prostate tumor in mice. The contrast agent resulted in improved tumor contrast enhancement in male athymic nude mice bearing orthotopic PC3 prostate tumor xenograft at a dose of 0.03 mmol Gd/kg. The peptide targeted MRI contrast agent is promising for high-resolution MR molecular imaging of prostate tumor.

Introduction

Early accurate detection and diagnosis of malignant tumors enable more effective cancer treatment at an earlier stage, resulting in improved survival rate and quality of the life of cancer patients (1). Effective imaging of cancer related molecular targets is of great significance to improve the accuracy of earlier cancer detection and diagnosis. Molecular imaging has been proven successful for accurate cancer detection and rapid assessment of therapeutic efficacy with highly sensitive imaging modalities, including PET and SPECT (2–6). However, these imaging modalities cannot provide high resolution images of anatomic structures and are often combined with other anatomic imaging modalities, e.g. CT and MRI, to correlate molecular imaging with structural imaging for accurate diagnosis (7–10).

Correspondence to: Dr. Zheng-Rong Lu, Department of Biomedical Engineering, Wickenden Building, Room 427, Case Western Reserve University, 10900 Euclid Avenue, Cleveland, OH 44106-7207, zxl125@case.edu.

Magnetic resonance imaging (MRI) is a powerful clinical imaging modality with high spatial resolution and no ionization radiation. MRI provides both anatomical and physiological information of soft tissues (11,12). Contrast enhanced MRI can produce high-resolution image contrast between diseased tissue and normal tissue. Currently, no targeted contrast agent is available for clinical MR cancer molecular imaging. Innovative design and development of targeted MRI contrast agents would greatly advance the application of MR cancer molecular imaging. Significant efforts have been made on developing targeted contrast agents for MR imaging of the biomarkers expressed on the surface of cancer cells. Due to relatively low sensitivity of MRI and low concentration of these biomarkers, it is a challenge to generate sufficient contrast enhancement for effective MR molecular imaging using small molecular targeted contrast agents (13,14). In order to obtain sufficient enhancement, various delivery systems such as liposomes, nanoparticles and polymer conjugates with a high payload of paramagnetic Gd(III) chelates have been prepared to increase local concentration of contrast agents at the target sites (15–22). Although these delivery systems are able to generate significant tumor enhancement in animal models, their large sizes result in slow and incomplete elimination from the body, resulting in prolonged accumulation of toxic Gd(III) ions that can cause serious safety concerns and prevent further clinical development (23–26). Recently, some studies have shown that the limitations of MRI for molecular imaging can be overcome by selecting proper molecular biomarkers with high local expression in the lesion tissues and using small molecular agents that can be readily excreted (27–35). The key feature of these agents is that they target molecular markers abundantly present in the diseased tissues with little presence in normal tissues. A sufficient amount of contrast agents can bind to these targets, resulting in sufficient contrast enhancement for effective MR molecular imaging. Since their size is smaller than the renal filtration threshold, unbound contrast agents can readily be excreted from the body with reduced background noise.

Malignant tumors have a unique microenvironment that contains a meshwork of clotted proteins in the tumor stroma, but no such meshwork is detectable in normal tissues (36–40). The protein clots are formed by plasma proteins that leak into the extravascular space in tumors, presumably due to tumor angiogenesis and vascular hyperpermeability. We hypothesized that clotted plasma proteins in tumor stroma could be a viable target for MR cancer molecular imaging. Their abundance in the tumor stroma allows the binding of sufficient low molecular weight targeted contrast agents to generate MRI detectable contrast enhancement for effective cancer molecular imaging. Ruoslahti's group recently reported two cyclic peptides CGLIIQKNEC (CLT1) and CNAGESSKNC (CLT2) bound specifically to the clotted plasma proteins (fibrin-fibronectin complexes) formed in tumor stroma (39). We have recently demonstrated that CLT1-(DTPA-Gd) was effective to generate sufficient contrast enhancement for MR cancer molecular imaging in different tumor models, including MDA-MB-231 breast cancer and HT29 colon cancer (41,42). Although Gd-DTPA and its derivatives have been used in clinical practice, the linear Gd(III) chelates suffer from low kinetic stability against transmetallation with endogenous metal ions (43,44).

Macrocyclic Gd(III) chelates have high thermodynamic and kinetic stability with no transmetallation with endogenous metal ions (43–46). In this study, we designed and synthesized a new low molecular weight CLT1 targeted contrast agent based on a highly stable macrocyclic Gd(III) chelate, Gd-DOTA. The new CLT1 targeted contrast agent CLT1-dL-$(Gd\text{-}DOTA)_4$ had 4 Gd-DOTA monoamide chelates conjugated to a CLT1 molecule via a generation 1 lysine dendrimer. A corresponding scrambled CLT1 targeted agent was synthesized and used as a non-targeted control agent. The tumor specificity of CLT1 was determined in an orthotopic xenograft PC3 prostate tumor model in male athymic nude mice using fluorescence imaging. The effectiveness of CLT1-dL-$(Gd\text{-}DOTA)_4$ for MR molecular imaging of the prostate tumor was determined in the same tumor model.

Materials and Methods

1,4,7,10-Tetraazacyclododecane-1,4,7-tris-*tert*-butyl acetate-10-acetic acid [DOTA-tris(*t*-Bu)] was purchased from TCI America (Portland, OR, USA). Benzotriazol-1-yl-oxytripyrrolidinophosphonium hexafluorophosphate (PyBOP), 1-hydroxybenzotriazole hydrate (HOBt), and 2-(1*H*-benzotriazol-1-yl)-1,1,3,3-tetramethyl uronium hexafluorophosphate (HBTU) were purchased from Nova Biochem (Darmstadt, Germany). Fmoc protected amino acids and Fmoc-12-amino-4,7,10-trioxadodecanoic acid (Fmoc-NH-PEG-COOH, MW = 443.5) were purchased from EMD Chemicals Inc. (Gibbstown, NJ, USA). Anhydrous *N,N*-diisopropylethylamine (DIPEA), dichloromethane (DCM), and *N,N*-dimethylformamide (DMF) were purchased from Alfa Aesar (Ward Hill, MA, USA). Trifluoroacetic acid (TFA) was purchased from ACROS Organics (Morris Plains, NJ, USA). Thallium(III) trifluoroacetate and triisobutylsilane (TIS) were purchased from Sigma-Aldrich Corp. (St. Louis, MO, USA). Texas Red, succinimidyl ester, single isomer (T20175) was purchased from Invitrogen (Eugene, Oregon, USA). All reagents were used without further purification.

Synthesis of cyclic peptide CLT1 (CGLIIQKNEC)

Peptide CLT1 was synthesized using standard solid-phase peptide synthesis from Fmoc-protected amino acids on a 2-chlorotrityl chloride resin. 2-Chlorotrityl chloride resin (1.27g, 2.0 mmol, loading rate =1.58 mmol Cl/g) was suspended and swollen in anhydrous dichloromethane (DCM) (20 ml) and shaken for 1 h in an ISOLUTE column. The resin was then filtered and washed with anhydrous DCM (20 ml), and anhydrous dimethylformamide (DMF, 20 ml). Fmoc-Cys(Acm)-OH (414 mg, 1.0 mmol) was dissolved in DMF (10 ml) and added to the resin. N,N-Diisopropylethylamine (DIPEA, 800 μL) was added and the suspension was shaken for 2 h. The resin was then filtered and washed with DCM/DMF three times. The resin was further shaken with methanol/DIPEA (20 ml/800 μL) for 20 min to block the remaining active chloride on the resin. After washing with DCM/DMF, the Fmoc protecting group was removed with 20% piperidine in DMF (5 min×3, 20 ml/each). This procedure was repeated in the following order: Fmoc-Glu(O*t*Bu)-OH, Fmoc-Asn(Trt)-OH, Fmoc-Lys(Boc)-OH, Fmoc-Gln(Trt)-OH, Fmoc-Ile-OH, Fmoc-Ile-OH, Fmoc-Leu-OH, Fmoc-Gly-OH, Fmoc-Cys(Acm)-OH. Each Fmoc deprotection and amino acid coupling step was followed by a Kaiser's test on resin. The resin in each reaction cycle was extensively washed with DCM/DMF and dried under reduced pressure before proceeding to next step. After adding final amino acid, on-resin cyclization of the linear peptide was carried out with thallium(III) trifluoroacetate (1.09 g, 2.0 mmol, 2 equivalents) in DMF (20 ml) at 0 °C for 2 h, followed by extensively washing with DMF/DCM. A sample of the dry resin was treated with a cocktail of trifluoroacetic acid (TFA), water, and triisobutylsilane (TIS) (2 mL, 95/2.5/2.5) and shaken for 1 h at room temperature to remove the protection groups and to cut the peptide from the resin. The filtered solution was dropped to cold ethyl ether (50 ml). A solid product was collected by centrifugation and washed with ether 4 times to give compound CLT1, which was characterized by MALDI-TOF [(*m/z*[M+H]$^+$): 1118.82 (obsd.), 1118.33 (calcd.)].

Synthesis of CLT1-dL-(DOTA)$_4$

After on-resin cyclization, PEG and lysine were sequentially conjugated to the N-terminus of CLT1 peptide (1.0 mmol) on resin by reacting with Fmoc-NH-PEG-COOH (3.0 mmol), Fmoc-Lys(Fmoc)-OH (3.0 mmol), and then another batch of Fmoc-Lys(Fmoc)-OH (6 mmol). After removal of Fmoc, DOTA-tris(t-Bu) (4.58 g, 8.0 mmol, 2 equivalents to each amino group) was reacted with the four free amines from the lysine dendrimer on the resin surface for 2 h. Finally, the product was deprotected and cleaved from the resin by treating with a cocktail of trifluoroacetic acid, water, and triisobutylsilane (20 mL, 95/2.5/2.5) and

shaken for 8 h at room temperature. The resin was removed by filtration and washed with TFA. Combined filtrates were added dropwise to cold ethyl ether (200 mL). The precipitated crude product was centrifuged, washed with ethyl ether 4 times, dried under vacuum to give a colorless solid (1.99 g, 61 % yield). The crude product were purified by preparative HPLC on an Agilent 1100 HPLC system equipped with a ZORBAX 300SB-C18 PrepHT column. The gradient of HPLC was 0–40% solvent B (0.1% TFA in acetonitrile) in solvent A (0.1% TFA aqueous solution) for 20 min and 40–90% solvent B in solvent A for 10 min. The purified product CLT1-dL-$(DOTA)_4$ was characterized by MALDI-TOF [(*m/z*[M+ H]$^+$): 3251.62 (obsd.), 3251.68 (calcd.)].

Synthesis of CLT1-dL-$(Gd\text{-}DOTA)_4$

CLT1-dL-$(DOTA)_4$ (250 mg, 0.077 mmol) was dissolved in DI water (15 ml), the pH was adjusted to 6 using 1 M NaOH. $Gd(OAc)_3.4H_2O$ (472 mg, 0.462 mmol, 1.5 equivalents to DOTA monoamide) was added in portions to the solution, while maintaining the pH at 6 using 1M NaOH. The reaction was stirred for 48 h at room temperature. The excess of $Gd(OAc)_3$ was used to ensure complete chelation. Residual Gd(III) was complexed with ethylenediaminetetraacetic acid (EDTA) (90 mg, 0.31 mmol), and the crude product was then purified by Sephadex G-10 column to give final product CLT1-dL-$(Gd\text{-}DOTA)_4$ (169 mg, 57 %). CLT1-dL-$(Gd\text{-}DOTA)_4$ was characterized by MALDI-TOF [(*m/z*[M+H]$^+$): 3869.85 (obsd.), 3869.53 (calcd.)].

Synthesis of scrambled CLT1-dL-$(Gd\text{-}DOTA)_4$

A scrambled CLT1 (CIEGNKIQLC, sCLT1) Gd-DOTA monoamide conjugate sCLT1-dL-$(Gd\text{-}DOTA)_4$ was synthesized using the similar procedure as CLT1-dL-$(Gd\text{-}DOTA)_4$. sCLT1-dL-$(Gd\text{-}DOTA)_4$ was characterized by MALDI-TOF [(*m/z*, [M+ H]$^+$): 3869.10 (obsd.), 3869.63 (calcd.)].

Synthesis of CLT1-Texas Red (TR) and scrambled sCLT1-TR conjugates

The peptides CLT1 and sCLT1 were first synthesized using standard solid-phase peptide chemistry as described above. Fluorescence dye Texas Red (2 mg) was then conjugated to the peptides on resin (10 mg) in the presence of coupling agents. After cleaved from the resin with an acidic cocktail of TFA:water:TIS (95:2.5:2.5), the products CLT1-TR and sCLT1-TR were purified by preparative HPLC using the same separation protocol as above. Molecular weight of the conjugates was determined by MALDI-TOF [(*m/z*[M+H]$^+$): 2023.05 (obsd.), 2023.41 (calcd.); (*m/z*[M+Na]$^+$): 2045.61 (obsd.), 2045.41 (calcd.)]. sCLT1-TR conjugate was similarly prepared. sCLT1-TR was also characterized by MALDI-TOF [(*m/z*[M+H]$^+$): 2022.75 (obsd.); (*m/z*[M+Na]$^+$): 2045.89 (obsd.)].

Characterization of purified compounds

The Gd(III) content was measured by inductively coupled plasma-optical emission spectroscopy (ICP-OES Optima 3100XL, Perkin-Elmer, Norwalk, CT). Matrix-assisted laser desorption/ionization time-of-flight (MALDI-TOF) mass spectra were acquired on a MALDI-TOF mass spectrometer (AutoflexTM Speed, Bruker) in a linear mode with 2,5-dihydroxybenzoic acid (2,5-DHB) as a matrix. Relaxation times of the aqueous solution of the contrast agents of CLT1-dL-$(Gd\text{-}DOTA)_4$ and sCLT1-dL-$(Gd\text{-}DOTA)_4$ with different concentrations were measured at 60 MHz (1.5 T) using a Bruker minispec relaxometer at 37 °C. T_1 was measured with an inversion–recovery pulse sequence. T_2 was measured using a Carr-Purcell-Meiboom-Gill sequence with 500 echoes collected. The T_1 and T_2 relaxivities of the agents were calculated from the slopes of the plots of $1/T_1$ and $1/T_2$ versus the Gd concentrations.

Animal model with orthotopic PC3 prostate tumor

Male NIH athymic nude mice (4–5 weeks old) were maintained at the Athymic Animal Core Facility at Case Western Reserve University according to an animal protocol approved by the CWRU Institutional Animal Care and Use Committee. PC3 prostate cancer cells with constitutive expression of green fluorescence protein (GFP) were cultured in RPMI medium supplemented with 5% fetal bovine serum and penicillin/streptomycin/fungizone, harvested by trypsinization and resuspended at density of 2.5×10^4 cells per 1.0 μL PBS. The mice were anesthetized and a small incision was made through the skin and peritoneum along the lower midline for about 1 cm. The prostate dorsal lobes were gently exteriorized and stabilized. The suspension of PC3-GFP cells in PBS (20 μl) was injected into the prostate with a 30-gauge needle. Finally the incision was closed with wound autoclip (47).

Tumor binding specificity of the peptides

Before injection of the peptide probes, GFP fluorescence images with live mice were acquired to verify the tumor presence. Texas Red labeled peptides were intravenously injected to the tumor bearing mice at a dose of 10 nmol/mouse. After 2 h, the mice were sacrificed, and the tumors and major organs were collected and imaged immediately on a Maestro fluorescence imager. GFP fluorescence images were obtained using green light filters for GFP (excitation: 444–490 nm; emission: 515 nm long-pass filter; acquisition settings: 500–720 in 10 nm steps) and red light filters for Texas Red labeled probes (excitation: 576–621 nm; emission: 635 nm long-pass filter; acquisition settings: 630–800 in 10 nm steps). Exposure time was 10 ms for GFP and 150 ms for Texas Red.

Histology studies

Immediately after measurement of whole tissue fluorescence imaging, tumor tissues were collected and cryosectioned into 5-μm slices. After rinsed with PBS, 1 drop of UltraCruz™mounting medium (sc-24941, Santa Cruz Biotechnology, Inc. Santa Cruz, CA, USA) containing 4’,6-diamidino-2-phenylindole (DAPI) was mounted and imaged immediately on an Olympus FV1000 confocal laser scanning microscope.

MR tumor molecular imaging

The MRI study was performed on a Bruker Biospec 7 T MRI scanner (Bruker Corp., Billerica, MA, USA) with a volume radio frequency (RF) coil. Mice were anesthetized with a 2% isoflurane-oxygen mixture in an isoflurane induction chamber. A tail vein of mouse was catheterized with a 30 gauge needle connected with a 2.5 m long tubing filled with heparinized saline. The animal was then placed into the magnet and kept under inhalation anesthesia with 1.5% isoflurane-oxygen via a nose cone. A respiratory sensor connected to a monitoring system (SA Instruments, Stony Brook, NY) was placed on the abdomen to monitor rate and depth of respiration. The body temperature was maintained at 37°C by blowing hot air into the magnet through a feedback control system. A group of 6 mice was used for each agent. Sagittal section images were acquired with a localizing sequence to identify the tumor location, followed by a 2D T_1-weighted gradient fat suppression sequence before injection. After pre-injection baseline MR image acquisition, the targeted agent or control agent was injected at a dose of 0.03 mmol of Gd/kg by flushing with 200 μL of saline. T_1-weighted 2D axial images were then acquired at different time points after the injection for up to 30 min. Parameters of the 2D T_1-weighted gradient echo sequence were TR/TE = 151.2/1.9 ms, FOV = 3.0 cm, slice thickness = 1.2 mm, slice number = 20, average = 1, flip angle = 80°, matrix = 128 ×128. In order to acquire the images of the tumor and kidneys, 20 slices were acquired to cover the whole tumor and the kidneys. MR images of the kidneys were also acquired at 48 h after injection.

Image processing and analysis

Image analysis was performed using Bruker ParaVision 4.0 imaging software. Regions of interest (ROIs) were drawn over the whole tumor and the kidneys in the two-dimensional imaging plane and average signal intensity was measured. Tumor or kidney contrast enhancement (ΔSNR) was calculated as post-contrast SNR increase over pre-contrast SNR using the following equation: $\Delta SNR = (S_t/\sigma_t) - (S_0/\sigma_0)$, where S_0 and S_t denoted the signal in tumor or the kidneys before and after contrast, σ_0 and σ_t were the standard deviation of noise measured from the background air before and after contrast. The p values were calculated using the student's two-tailed t-test, assuming statistical significance at $p < 0.05$.

Biodistribution study

The mice from the MRI study were sacrificed by cervical dislocation at 48 h post-injection. The organ and tissue samples, including the heart, liver, spleen, lung, kidneys, brain, skin, muscle, femur, and tumor were collected and weighed. The tissue samples were then cut into small pieces and mixed with ultra-pure nitric acid (1.0 ml, 70%, EMD, Gibbstown, NJ). The tissue samples were liquefied for 1 week, and the solution was transferred to a centrifuge tube and centrifuged at 14,000 rpm for 5 min. The supernatant (0.2 ml) was diluted 10 times with de-ionized water and further centrifuged at 14,000 rpm for 5 min. The Gd(III) concentration in the supernatant solution was measured by ICP-OES. The average Gd(III) content in each organ or tissue was calculated from the measured Gd(III). The Gd content was calculated as the percentage of injected dose per gram of organ/tissues (% ID/g).

Results

Synthesis and Characterization

The synthesis of CLT1 peptide targeted Gd-DOTA monoamide conjugate, CLT1-dL-(Gd-DOTA)$_4$, is described in Scheme 1. A generation 1 lysine dendrimer was used to increase the molar ratio of Gd-DOTA monoamide to the peptide in the targeted contrast agent for effective targeted contrast enhancement. The small size of G1 lysine dendrimer would allow the unbound contrast agent to rapidly excrete from the body via renal filtration. The lysine dendrimer also had a neutral core, which could minimize charge-associated non-specific tissue uptake. The conjugation of multiple Gd-DOTA monoamide chelates to each CLT1 peptide resulted in a final product with good water solubility. The peptide and lysine dendrimer were connected via a short PEG linker to avoid steric hindrance for target binding. sCLT1 (CIEGNKIQLC) was used to prepare the non-targeted control agent. sCLT1-dL-(Gd-DOTA)$_4$ was similarly synthesized as described in Scheme 1. The final products were characterized by MALDI-TOF mass spectrometry (Figure 1), ICP-OES and Bruker minispec relaxometer. Figure 2 shows the plots of the T_1 and T_2 water proton relaxation rates versus the concentration of CLT1-dL-(Gd-DOTA)$_4$ and sCLT1-dL-(Gd-DOTA)$_4$ at 1.5 T (60 MHz), 37 °C. The physicochemical parameters of the contrast agents are listed in Table 1. Both targeted and scrambled agents had similar relaxivity. At 1.5 T, the T_1 relaxivity per gadolinium of CLT1-dL-(Gd-DOTA)$_4$ in pH 7.4 PBS was about 3 times higher than that of Gd-DOTA (48). Synthesis of CLT1-TR and sCLT1-TR was confirmed by MALDI-TOF mass spectrometry.

Tumor binding specificity of CLT1 peptide

Figure 3 (A,B) shows the bright field images and fluorescence images of tumors and major organs that were collected from mice injected with CLT1-TR and sCLT1-TR fluorescence probes. The GFP expressing tumors showed strong green fluorescence. Texas Red labeled CLT1 demonstrated strong binding to tumor, while the non-specific scrambled peptide resulted in little tumor binding. Both peptides showed little binding to the normal organs and

tissues. Figure 3C shows red fluorescence intensity extracted from the orthotopic prostate tumors of the mice injected with CLT1-TR and sCLT1-TR. The targeted CLT1-TR1 showed 5.7 times higher binding to the tumor tissue than non-targeted sCLT1-TR.

Figure 4 shows the microscopic fluorescence images of the tumor sections from these mice injected with CLT1-TR and sCLT1-TR. Blue fluorescence was from DAPI bound to the DNA in cell nuclei. Both tumor sections showed strong green fluorescence from GFP. Strong red fluorescence of Texas Red was shown in the tumor section obtained from the mice injected with CLT1-TR, while no fluorescence was essentially detected in tumor section from the mice injected with sCLT1-TR. The merged low-resolution fluorescent images (yellow color) exhibited good correlation of the green fluorescence from the tumor cells to the red fluorescence from CLT1-TR in the vicinity of the cells, indicating strong binding of the probe to viable tumor regions after intravenous administration.

MR tumor molecular imaging with CLT1-dL-(Gd-DOTA)$_4$

Figure 5 shows the representative 2D axial T_1-weighted gradient echo tumor images of the mice bearing orthotopic human PC3 prostate tumor before and after injection of CLT1-dL-(Gd-DOTA)$_4$ and sCLT1-dL-(Gd-DOTA)$_4$ at a dose of 0.03 mmol-Gd/kg. The targeted agent resulted in greater and longer enhancement in tumor tissue compared to non-targeted scrambled agents. Contrast enhancement in the urinary bladder gradually increased over time, indicating that the unbound contrast agents were excreted via renal filtration. Quantitative signal analysis revealed that the targeted agent produced more significant signal enhancement in the tumor tissue than the control agent ($p<0.05$) up to 30 minutes. CLT1-dL-(Gd-DOTA)$_4$ resulted in approximately 110 % more signal enhancement than sCLT1-dL-(Gd-DOTA)$_4$ in the tumor tissue at 1 minute post-injection. The signal enhancement gradually decreased over time and about 60 % more signal enhancement was still observed for the targeted agent than the control agent at 30 minutes post-injection.

Figure 6B shows the contrast enhancement in the kidneys up to 48 h after injection of the agents. Both agents showed similar dynamic kidney enhancement patterns, whereby strong contrast enhancement was observed at early time points after injection, followed by a rapid signal decrease, indicating rapid washout of the agents in the kidneys. Little enhancement was observed in the kidneys at 48 h after injection.

Biodistribution in mice

Figure 7 shows the biodistribution of Gd(III) in the major organs and tissues, including the femur, heart, kidneys, liver, lung, muscle, and spleen of mice 48 h after receiving CLT1-dL-(DOTA-Gd)$_4$ and sCLT1-dL-(DOTA-Gd)$_4$ at a dose of 0.03 mmol-Gd/kg. The Gd retention of both agents was comparable ($p > 0.05$) in the main normal organs and tissues, except kidneys, femur and tumor ($p < 0.05$) at 48 hours after the injection. Approximately 0.5 %, 0.8 % and 1.3 % of injected targeted CLT1-dL-(DOTA-Gd)$_4$ per gram of tissue was measured in the liver, spleen and kidneys, while very little (less than 0.1 %) or no Gd was measured in other tissues and organs.

Discussion

Currently, nuclear medicine is routinely used for cancer molecular imaging in clinical practice. Dual imaging modalities are often needed to co-register molecular imaging with anatomical imaging due to the poor spatial resolution of nuclear medicine. It would be ideal to use a single imaging modality for effective molecular and anatomic imaging to reduce unnecessary exposure to ionizing radiation, as well as the cost of the diagnosis. MRI is advantageous due to its high spatial resolution of soft tissues and the absence of ionizing

radiation. The key for effective clinical MR cancer molecular imaging is the design and development of safe effective targeted MRI contrast agents. This study has shown that it is possible to achieve effective MR cancer molecular imaging by utilizing a small molecular targeted contrast agent that binds properly selected molecular targets. Small size of the targeted MRI contrast agents is critical to allow the unbound targeted agent to rapidly excrete from the body via renal filtration and to minimize potential toxic side effects associated with Gd(III) based contrast agents. Tumor stroma has abundant local expression of cancer-related proteins, which could be suitable biomarkers for effective MR cancer molecular imaging. Their abundance expression in tumor stroma allows the binding of sufficient small molecular Gd(III) based contrast agents to generate robust contrast enhancement and to overcome the low sensitivity of MRI. Both thermodynamic and kinetic stability of the Gd(III) chelates should be considered in the design of new targeted agents to avoid the release of free Gd(III) ions and potential toxic side effects.

Previous studies have shown that the CLT1 peptide specifically bound to clotted plasma proteins, fibrin-fibronectin complexes, that are abundantly expressed in the stroma of many different tumors, including Lewis lung carcinoma (38,39), MDA-MB-231 breast cancer and HT29 colon cancer (41,42,49). In this study, we further verified the specific binding of CLT1 peptide to the orthotopic prostate PC-3 tumor tissue using in vivo fluorescence imaging. The peptide was highly specific to prostate tumor tissue and with little non-specific binding to normal tissues.

Numerous studies have demonstrated that macrocyclic chelate Gd-DOTA and its derivatives have higher kinetic stability than Gd-DPTA against transmetallation with endogenous metal ions, particularly Zn^{2+} ions (44–46). CLT1-dL-(Gd-DOTA)$_4$ should have high kinetic stability compared to previously reported linear CLT1-(Gd-DTPA) conjugate (41). The conjugation of multiple Gd-DOTA chelates to each CLT1 improved the water solubility of the peptide and the final product. The small molecular CLT1-dL-(Gd-DOTA)$_4$ generated significant contrast enhancement at a reduced dose of 0.03 mmol/kg. The tumor contrast enhancement was comparable to our previously reported CLT1 targeted nanoglobular contrast agents at the same dose (50). The results indicate that MRI with the small molecular targeted contrast agent is effective for high-resolution anatomic and molecular imaging of the abundant cancer-related biomarkers in tumor stroma. Our previous study showed that the tumor enhancement with CLT1 peptide targeted contrast agent CLT1-(Gd-DTPA) was reduced after the coinjection of free CLT1 peptide, indicating that the free peptide competitively recognizes the same binding site within tumor tissue as the CLT1 peptide targeted contrast agent (41). Due to the abundance of clotted plasma proteins in the tumor stroma, sufficient targeted contrast agent can bind to the molecular target. Consequently, the targeted agent overcomes the relative low sensitivity of contrast enhanced MRI, resulting in improved contrast enhancement for effective cancer molecular imaging at a reduced dose. MR molecular imaging of the clotted plasma proteins is advantageous over nuclear medicine for the same molecular targets because of its high anatomical resolution and the absence of ionizing radiation. Furthermore, no dual imaging modalities are needed to co-register molecular imaging with anatomic imaging.

As compared to macromolecules, the small peptide targeted contrast agent has a small size and can readily diffuse into tumor tissues for effective cancer molecular imaging. The small size also allows unbound contrast agents to be excreted from the body via renal filtration to reduce background signal and minimize the accumulation of Gd(III) chelates in the body. Complete elimination of the Gd(III) based MRI contrast agents from the body is critical for minimizing the safety concerns related to their slow excretion. According to a previous report (51), peptides may generally be reabsorbed by renal tubular cells. Here, the contrast enhanced MRI study showed that the targeted contrast agent excreted rapidly through the

kidneys into the urinary bladder. The kidneys had strong contrast enhancement at early time points after injection and the enhancement gradually decreased over time (Figure 6B), while strong contrast enhancement was observed in the urinary bladder within 15 minutes after injection of both agents (Figure 5). The results indicated that the peptide targeted agent could be readily excreted through the kidneys with minimal renal accumulation. The biodistribution studies also showed the agent had minimal Gd retention in the main organs and tissues 2 days after injection, much slower than our previously reported a high generation nanoglobular targeted MRI contrast agent (49). CLT1-dL-(Gd-DOTA)$_4$ showed promising properties for safe and effective cancer molecular imaging. Nevertheless, comprehensive toxicological evaluations are also required before further development of the agent for clinical cancer molecular imaging with MRI.

In summary, this study has validated the feasibility of CLT1 targeted small molecular contrast agent containing highly stable macrocyclic Gd(III) chelates for effective MR molecular imaging of biomarkers in the stroma of prostate tumor. The peptide targeted contrast agent has shown a great potential for accurate and earlier detection of small malignant tumors with contrast enhanced MRI. MR cancer molecular imaging with the targeted agent also has a potential for cancer grading and prognosis.

Acknowledgments

This work is supported in part by the NIH R01 CA097465. This material is based upon work supported by the National Science Foundation under Grant No. MRI-0821515 (for the purchase of the MALDI-TOF/TOF). We highly appreciate Dr. Wen Li and Dr. Vikas Gulani for MRI protocol test and setup, and Mr. Yvonne Parker for his assistance on tumor implantation.

References

1. Vlastos G, Verkooijen HM. Minimally invasive approaches for diagnosis and treatment of early-stage breast cancer. Oncologist. 2007; 12:1–10. [PubMed: 17227896]
2. Gelovani JG. Molecular imaging of epidermal growth factor receptor expression-activity at the kinase level in tumors with positron emission tomography. Cancer Metastasis Rev. 2008; 27:645–653. [PubMed: 18626573]
3. Piwnica-Worms D, Kesarwala AH, Pichler A, Prior JL, Sharma V. Single photon emission computed tomography and positron emission tomography imaging of multi-drug resistant P-glycoprotein--monitoring a transport activity important in cancer, blood-brain barrier function and Alzheimer's disease. Neuroimaging Clin N Am. 2006; 16:575–589. [PubMed: 17148020]
4. Hayashi M, Murakami K, Oyama T, Domeki Y, Hagiwara S, Katsumata D, Sunagawa M. PET/CT supports breast cancer diagnosis and treatment. Breast Cancer. 2008; 15:224–230. [PubMed: 18465196]
5. Saga T, Koizumi M, Furukawa T, Yoshikawa K, Fujibayashi Y. Molecular imaging of cancer: evaluating characters of individual cancer by PET/SPECT imaging. Cancer Sci. 2009; 100:375–381. [PubMed: 19154408]
6. Oude Munnink TH, Nagengast WB, Brouwers AH, Schroder CP, Hospers GA, Lub-de Hooge MN, van der Wall E, van Diest PJ, de Vries EG. Molecular imaging of breast cancer. Breast. 2009; 18(Suppl 3):S66–S73. [PubMed: 19914546]
7. Pan T, Mawlawi O. PET/CT in radiation oncology. Med. Phys. 2008; 35:4955–4966. [PubMed: 19070229]
8. Lucignani G. PET-MRI synergy in molecular, functional and anatomical cancer imaging. Eur. J. Nucl. Med. Mol. Imaging. 2008; 35:1550–1553. [PubMed: 18481060]
9. Maurer AH. Combined imaging modalities: PET/CT and SPECT/CT. Health Phys. 2008; 95:571–576. [PubMed: 18849691]
10. Lijowski M, Caruthers S, Hu G, Zhang H, Scott MJ, Williams T, Erpelding T, Schmieder AH, Kiefer G, Gulyas G, Athey PS, Gaffney PJ, Wickline SA, Lanza GM. High sensitivity: high-

resolution SPECT-CT/MR molecular imaging of angiogenesis in the Vx2 model. Invest. Radiol. 2009; 44:15–22. [PubMed: 18836386]

11. Haacke, EM.; Brown, RW.; Thompson, MR.; Venkatesan, R. Magnetic Resonance Imaging Physical Principles and Sequence Design. New York: John Wiley & Sons, Inc.; 1999.
12. Brown, MA.; Semelka, RC. MRI Basic Principles and Applications. 3rd Edition. Hoboken, New Jersey: John Wiley & Sons, Inc.; 2003.
13. Artemov D. Molecular magnetic resonance imaging with targeted contrast agents. J. Cell. Biochem. 2003; 90:518–524. [PubMed: 14523986]
14. Kalber TL, Kamaly N, So PW, Pugh JA, Bunch J, McLeod CW, Jorgensen MR, Miller AD, Bell JD. A low molecular weight folate receptor targeted contrast agent for magnetic resonance tumor imaging, Mol. Imaging Biol. 2011; 13 653-562.
15. Unger EC, Totty WG, Neufeld DM, Otsuka FL, Muephy WA, Welch MS, Connett JM, Philpott GW. Magnetic resonance imaging using gadolinium labeled monoclonal antibody. Invest. Radiol. 1985; 20:693–700. [PubMed: 4066240]
16. Schmieder AH, Winter PM, Caruthers SD, Harris TD, Williams TA, Allen JS, Lacy EK, Zhang H, Scott MJ, Hu G, Robertson JD, Wickline SA, Lanza GM. Molecular MR imaging of melanoma angiogenesis with alphanubeta3-targeted paramagnetic nanoparticles. Magn Reson Med. 2005; 53:621–627. [PubMed: 15723405]
17. Mulder WJ, Strilkers GJ, Griffioen AW, van Bloois L, Molema G, Storm G, Koning GA, Nicolay K. A liposomal system for contrast-enhanced magnetic resonance imaging of molecular targets. Bioconjug. Chem. 2004; 15:799–806. [PubMed: 15264867]
18. Lipinski MJ, Amirbekian V, Frias JC, Aguinaldo JG, Mani V, Briley-Saebo KC, Fuster V, Fallon JT, Fisher EA, Fayad ZA. MRI to detect atherosclerosis with gadolinium-containing immunomicelles targeting the macrophage scavenger receptor. Magn Reson Med. 2006; 56:601–610. [PubMed: 16902977]
19. Lanza GM, Winter PM, Caruthers SD, Morawski AM, Schmieder AH, Crowder KC, Wickline SA. Magnetic resonance molecular imaging with nanoparticles. J. Nucl. Cardiol. 2004; 11:733–743. [PubMed: 15592197]
20. Anderson SA, Rader RK, Westlin WF, Null C, Jackson D, Lanza GM, Wickline SA, Kotyk JJ. Magnetic resonance contrast enhancement of neovasculature with alpha(v)beta(3)-targeted nanoparticles. Magn. Reson. Med. 2000; 44:433–439. [PubMed: 10975896]
21. Amirbekian V, Lipinski MJ, Briley-Saebo KC, Amirbekian S, Aguinaldo JG, Weinreb DB, Vucic E, Frias JC, Hyafil F, Mani V, Fisher EA, Fayad ZA. Detecting and assessing macrophages in vivo to evaluate atherosclerosis noninvasively using molecular MRI. PNAS. 2007; 104:961–966. [PubMed: 17215360]
22. Mulder WJ, Strijkers GJ, Habets JW, Bleeker EJ, van der Schaft DW, Storm G, Koning GA, Griffioen AW, Nicolay K. MR molecular imaging and fluorescence microscopy for identification of activated tumor endothelium using a bimodal lipidic nanoparticle. FASEB J. 2005; 19:2008–2010. [PubMed: 16204353]
23. Franano FN, Edwards WB, Welch MJ, Brechbiel MW, Gansow OA, Duncan JR. Biodistribution and metabolism of targeted and nontargeted protein-chelate-gadolinium complexes: evidence for gadolinium dissociation in vitro and *in vivo*. Magn. Reson. Imaging. 1995; 13:201–214. [PubMed: 7739361]
24. Wang SJ, Brechbiel M, Wiener EC. Characteristics of a new MRI contrast agent prepared from polypropyleneimine dendrimers, generation 2. Invest. Radiol. 2003; 38:662–668. [PubMed: 14501494]
25. Bryant LH Jr, Jordan EK, Bulte JW, Herynek V, Frank JA. Pharmacokinetics of a high-generation dendrimer-Gd-DOTA. Acad. Radiol. 2002; 9(S1):S29–S33. [PubMed: 12019888]
26. Helbich TH, Gossman A, Mareski PA, Raduchel B, Roberts TP, Shames DM, Muhler M, Turetschek K, Brasch RC. A new polysaccharide macromolecular contrast agent for MR imaging: biodistribution and imaging characteristics. J. Magn. Reson. Imaging. 2000; 11:694–701. [PubMed: 10862070]
27. Burtea C, Laurent S, Murariu O, Rattat D, Toubeau G, Verbruggen A, Vansthertem D, Vander EL, Muller RN. Molecular imaging of $\alpha_v \beta_3$ integrin expression in atherosclerotic plaques with a

mimetic of RGD peptide grafted to Gd-DTPA. Cardiovasc. Res. 2008; 78:148–157. [PubMed: 18174291]

28. Botnar RM, Buecker A, Wiethoff AJ, Parsons EC, Katoh M Jr, Katsimaglis G, Weisskoff RM, Lauffer RB, Graham PB, Gunther RW, Manning WJ, Spuentrup E. In vivo magnetic resonance imaging of coronary thrombosis using a fibrin-binding molecular magnetic resonance contrast agent. Circulation. 2004; 110:1463–1466. [PubMed: 15238457]
29. Spuentrup E, Katoh M, Wiethoff AJ, Parsons EC Jr, Botnar RM, Mahnken AH, Gunther RW, Buecker A. Molecular magnetic resonance imaging of pulmonary emboli with a fibrin-specific contrast agent. Am. J. Respir. Crit. Care Med. 2005; 172:494–500. [PubMed: 15937292]
30. Overoye-Chan K, Koerner S, Looby RJ, Kolodziej AF, Zech SG, Deng Q, Chasse JM, McMurry TJ, Caravan P. EP-2104R: a fibrin-specific gadolinium-Based MRI contrast agent for detection of thrombus. J. Am. Chem. Soc. 2008; 130:6025–6039. [PubMed: 18393503]
31. Spuentrup E, Botnar RM, Wiethoff AJ, Ibrahim T, Kelle S, Katoh M, Ozgun M, Nagel E, Vymazal J, Graham PB, Gunther RW, Maintz D. MR imaging of thrombi using EP-2104R, a fibrin-specific contrast agent: initial results in patients. Eur. Radiol. 2008; 18:1995–2005. [PubMed: 18425519]
32. Spuentrup E, Ruhl KM, Botnar RM, Wiethoff AJ, Buhl A, Jacques V, Greenfield MT, Krombach GA, Gunther RW, Vangel MG, Caravan P. Molecular magnetic resonance imaging of myocardial perfusion with EP-3600, a collagen-specific contrast agent: initial feasibility study in a swine model. Circulation. 2009; 119:1768–1775. [PubMed: 19307474]
33. Caravan P, Das B, Dumas S, Epstein FH, Helm PA, Jacques V, Koerner S, Kolodziej A, Shen L, Sun WC, Zhang Z. Collagen-targeted MRI contrast agent for molecular imaging of fibrosis. Angew. Chem. Int. Ed. Engl. 2007; 46:8171–8173. [PubMed: 17893943]
34. Amirbekian V, Aguinaldo JG, Amirbekian S, Hyafil F, Vucic E, Sirol M, Weinreb DB, Le Greneur S, Lancelot E, Corot C, Fisher EA, Galis ZS, Fayad ZA. Atherosclerosis and matrix metalloproteinases: experimental molecular MR imaging in vivo. Radiology. 2009; 251:429–438. [PubMed: 19224894]
35. Boutry S, Burtea C, Laurent S, Toubeau G, Vander Elst L, Muller RN. Magnetic resonance imaging of inflammation with a specific selectin-targeted contrast agent. Magn. Reson. Med. 2005; 53:800–807. [PubMed: 15799062]
36. Abe K, Shoji M, Chen J, Bierhaus A, Danave I, Micko C, Casper K, Dillhay DL, Nawroth PP, Rickles FR. Regulation of vascular endothelial growth factor production and angiogenesis by the cytoplasmic tail of tissue factor. Proc. Natl. Acad. Sci. U.S.A. 1999; 96:8663–8668. [PubMed: 10411932]
37. Zhang J, Ding J, Zhang X, Shao X, Hao Z. Regulation of vascular endothelial growth factor (VEGF) production and angiogenesis by tissue Factor (TF) in SGC-7901 gastric cancer cells. Cancer Biol. Ther. 2005; 4:769–772. [PubMed: 15846107]
38. Ruoslahti E. Specialization of tumour vasculature. Nat. Rev. Cancer. 2002; 2:83–90. [PubMed: 12635171]
39. Pilch J, Brown DM, Komatsu M, Jarvinen TA, Yang M, Peters D, Hoffman RM, Ruoslahti E. Peptides selected for binding to clotted plasma accumulate in tumor stroma and wounds. Proc. Natl. Acad. Sci. U.S.A. 2006; 103:2800–2804. [PubMed: 16476999]
40. Simberg D, Duza T, Park JH, Essler M, Pilch J, Zhang L, Derfus AM, Yang M, Hoffman RM, Bhatia S, Sailor MJ, Ruoslahti E. Biomimetic amplification of nanoparticle homing to tumors. Proc. Natl. Acad. Sci. U.S.A. 2007; 104:932–936. [PubMed: 17215365]
41. Ye F, Wu X, Jeong EK, Jia Z, Yang T, Parker D, Lu Z-R. A peptide targeted contrast agent specific to fibrin-fibronectin complexes for cancer molecular imaging with MRI. Bioconjug. Chem. 2008; 19:2300–2303. [PubMed: 19053180]
42. Ye F, Jeong EK, Parker D, Lu Z-R. Evaluation of CLT1-(Gd-DTPA) for MR molecular imaging in a mouse breast cancer model. Chin. J. Magn. Reson. Imaging. 2011; 2:325–330.
43. Idée JM, Port M, Metdina C, Lancelot E, Fayoux E, Ballet S, Corot C. Possible involvement of gadolinium chelates in the pathophysiology of nephrogenic systemic fibrosis: a critical review. Toxicology. 2008; 248:77–88. [PubMed: 18440117]

44. Idée JM, Port M, Raynal I, Schaefer M, Le Greneur S, Corot C. Clinical and biological consequences of transmetallation induced by contrast agents for magnetic resonance imaging: a review. Fundam. Clin. Pharmacol. 2006; 20:563–576. [PubMed: 17109649]
45. White GW, Gibby WA, Tweedle MF. Comparison of Gd(DTPA-BMA) (Omniscan) versus Gd(HP-DO3A) (ProHance) relative to gadolinium retention in human bone tissue by inductively coupled plasma mass spectroscopy. Invest. Radiol. 2006; 41:272–278. [PubMed: 16481910]
46. Wu X, Zong Y, Ye Z, Lu Z-R. Stability and biodistribution of a biodegradable macromolecular MRI contrast agent Gd-DTPA cystamine copolymers (GDCC) in rats. Pharm. Res. 2010; 27:1390–1397. [PubMed: 20393871]
47. Burden-Gulley SM, Gates TJ, Burgoyn AM, Cutter JL, Lodowski DT, Robinson S, Sloan AE, Miller RH, Basilion JP, Brady-Kalnay SM. A novel molecular diagnostic of glioblastomas: detection of an extracellular fragment of protein tyrosine phosphatase mu. Neoplasia. 2010; 12:305–316. [PubMed: 20360941]
48. Rohrer M, Bauer H, Mintorovitch J, Requardt M, Weinmann HJ. Comparison of magnetic properties of MRI contrast media solutions at different magnetic field strengths. Invest. Radiol. 2005; 40:715–724. [PubMed: 16230904]
49. Tan M, Wu X, Jeong EK, Chen Q, Lu Z-R. Peptide-targeted Nanoglobular Gd-DOTA monoamide conjugates for magnetic resonance cancer molecular imaging. Biomacromolecules. 2010; 11:754–761. [PubMed: 20131758]
50. Tan M, Burden-Gulley S, Li W, Wu X, Lindner D, Brady-Kalnay S, Lu Z-R. MR Molecular Imaging of Prostate Cancer with a Peptide-Targeted Contrast Agent in a Mouse Orthotopic Prostate Cancer Model. Pharm. Res. 2012; 29:953–960. [PubMed: 22139536]
51. DeNardo SJ, O'Donnell RT, DeNardo GL. Potential use of amino acid cocktails to reduce renal tubular reabsorption of radioconjugates. J. Nucl. Med. 1996; 37:837–838. [PubMed: 8965156]

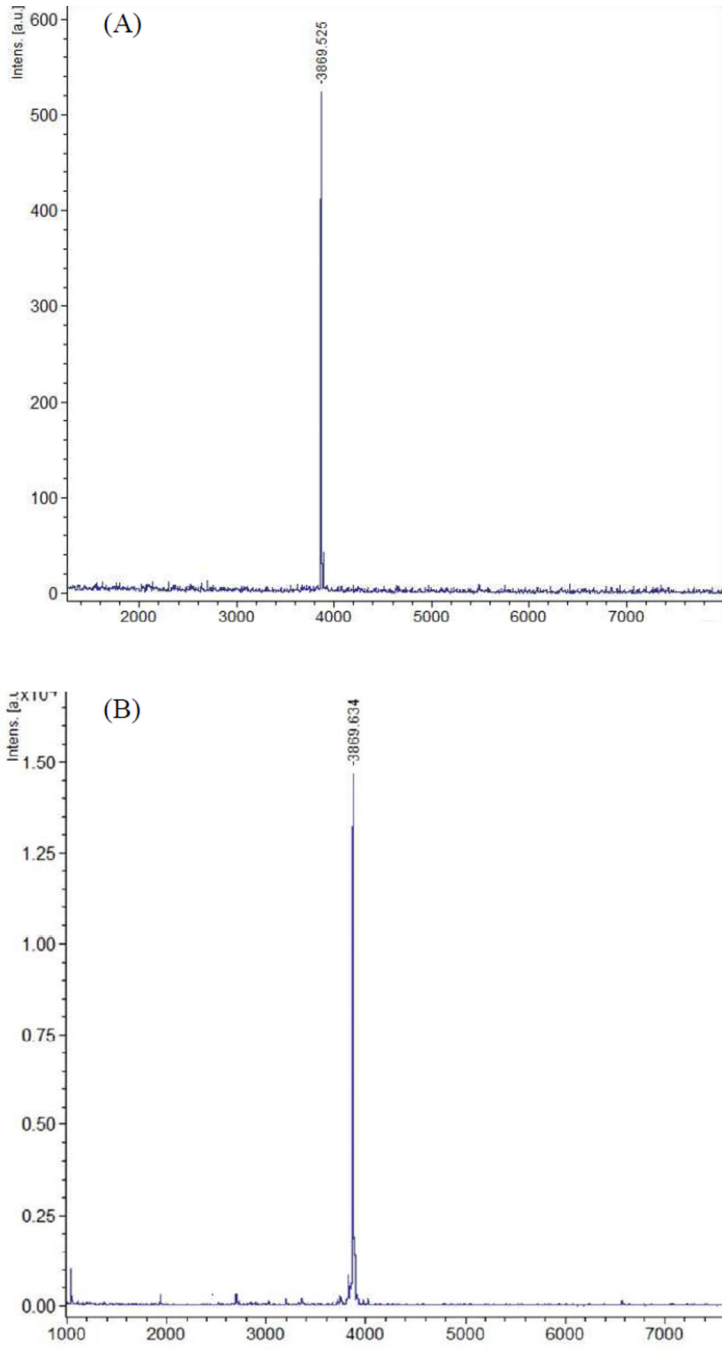

Figure 1.
MALDI-TOF mass spectra of CLT1-dL-(Gd-DOTA)$_4$ (A) and sCLT1-dL-(Gd-DOTA)$_4$ (B)

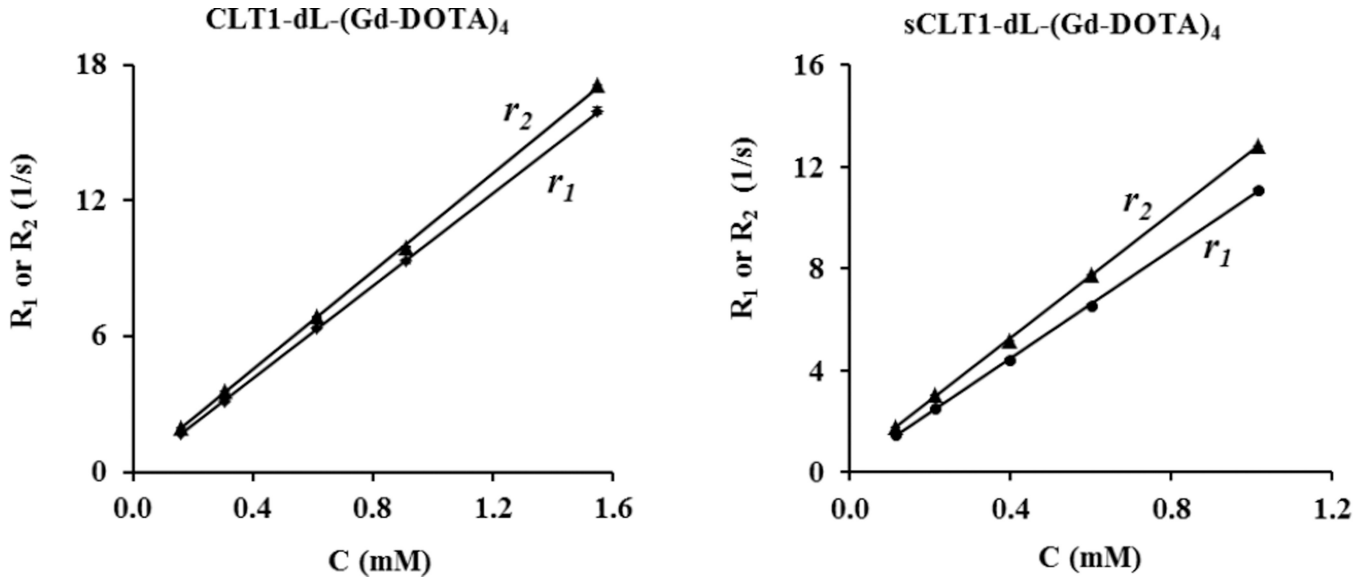

Figure 2.

Plots of $1/T_1$ (R_1) and $1/T_2$ (R_2) versus the concentration of the contrast agents CLT1-dL-$(Gd\text{-}DOTA)_4$ and sCLT1-dL-$(Gd\text{-}DOTA)_4$.

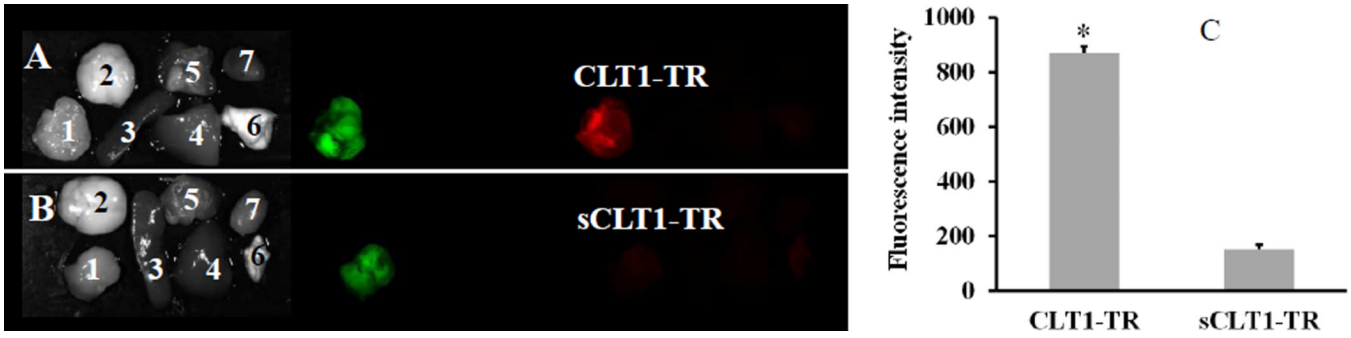

Figure 3.

Tumor binding of CLT1-TR (A) and sCLT1-TR (B) in athymic nude mice bearing orthotopic PC3-GFP prostate tumor 2 hours after intravenous injection at a dose of 10 nmol/mouse. CLT1-TR resulted in 5.7 times higher red fluorescence intensity in the tumor than sCLT1-TR (C, n = 3, * $p < 0.05$). 1. tumor; 2. brain; 3. spleen; 4. liver; 5. muscle; 6. lung; 7. heart.

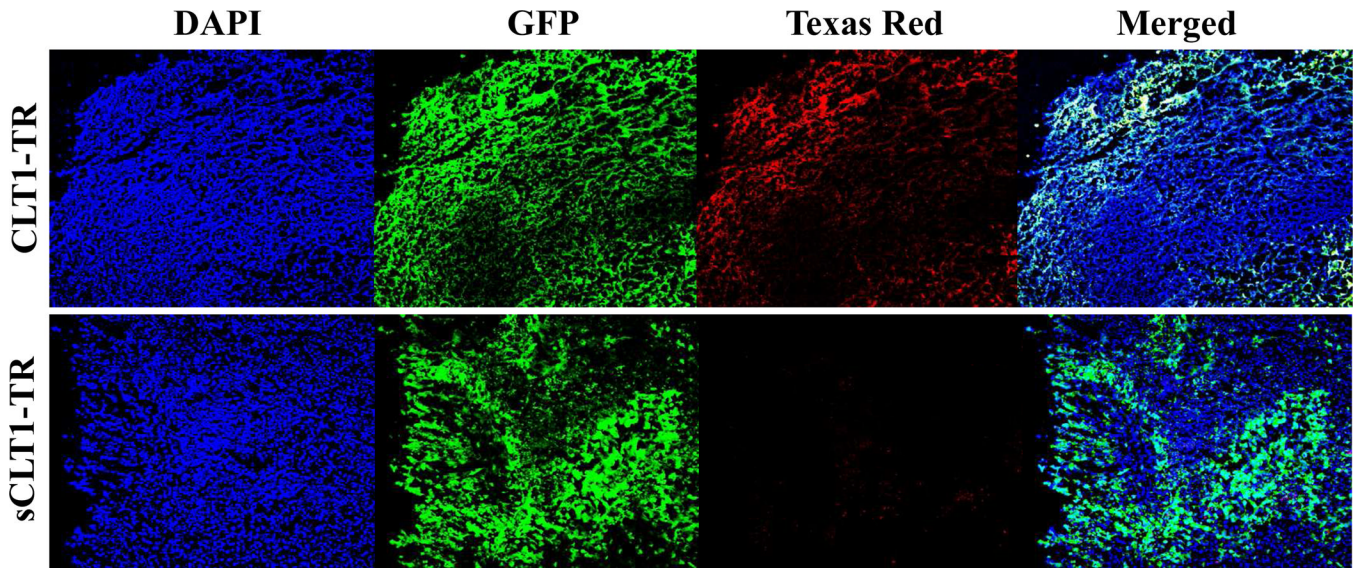

Figure 4.
Histological analysis of tumor tissue injected with CLT1-TR or sCLT1-TR at a dose of 10 nmol/mouse.

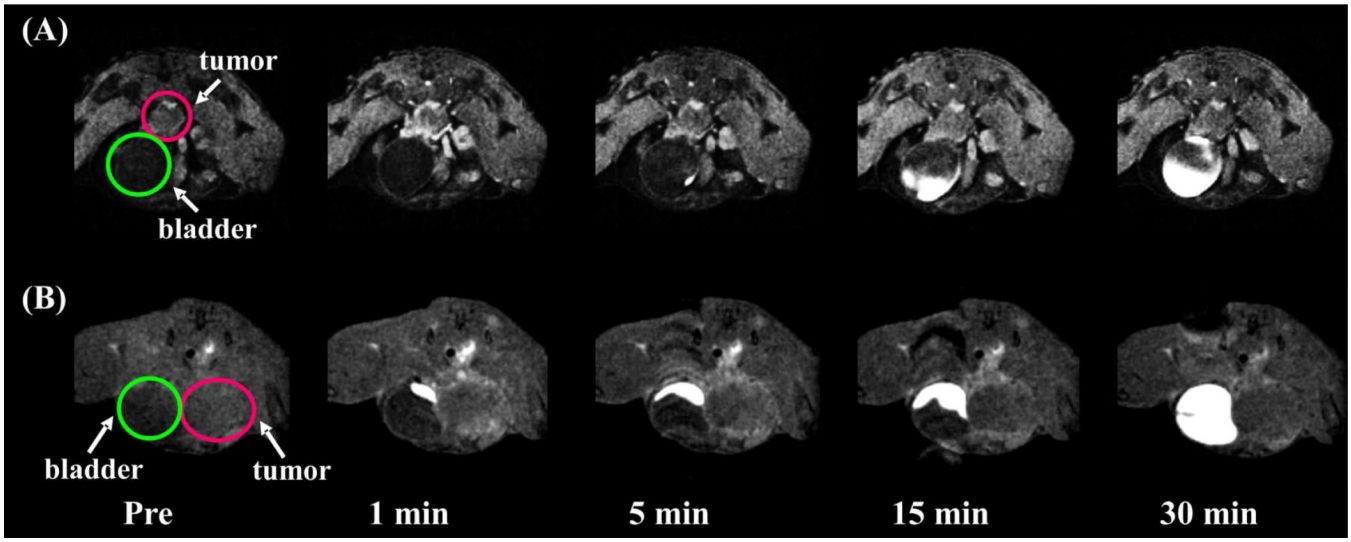

Figure 5.

Representative T_1-weighted axial 2D gradient images of orthotopic PC-3 human prostate tumor before and after intravenous injection of CLT1-dL-(Gd-DOTA)$_4$ (A) and sCLT1-dL-(Gd-DOTA)$_4$ (B) at 0.03 mmol Gd/kg in nu/nu mice. Tumor labeled with red circle and bladder labeled with green circle.

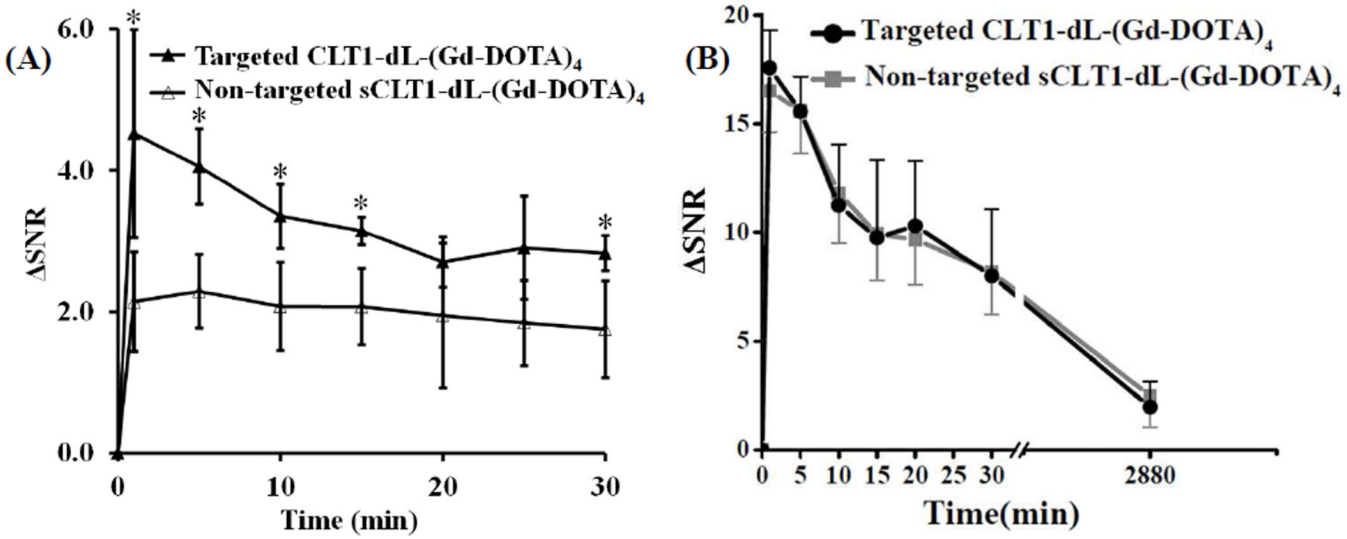

Figure 6.

Contrast enhancement (ΔSNR) in the tumor (A) and kidneys (B) produced by CLT1-dL-$(Gd\text{-}DOTA)_4$ and sCLT1-dL-$(Gd\text{-}DOTA)_4$ at 0.03 mmol-Gd/kg in nu/nu nude with athymic mice (n=6) bearing orthotopic human prostate tumor. * $p < 0.05$.

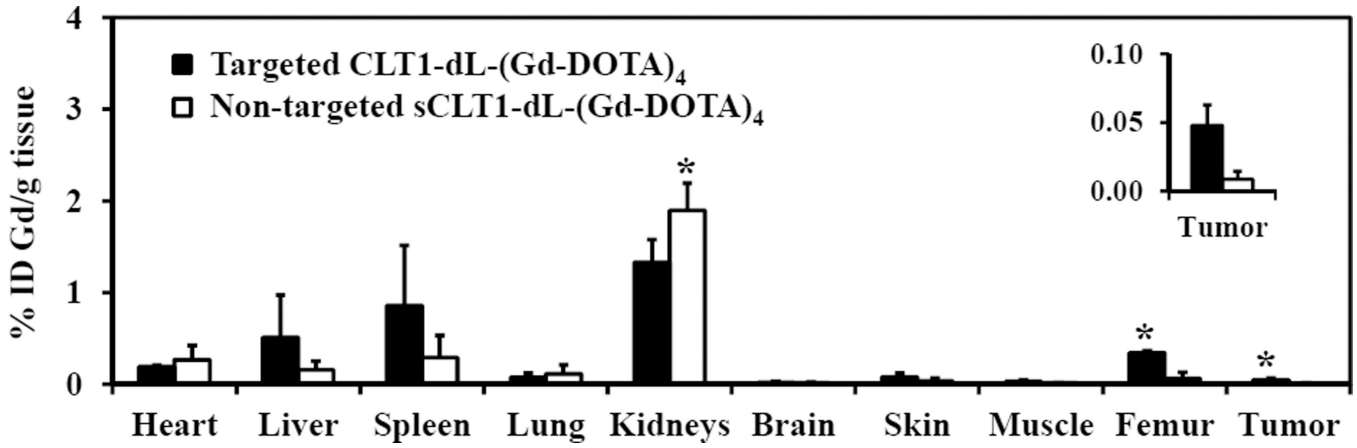

Figure 7.

Biodistribution of gadolinium in the major organs and tissues of mice at 48 h after intravenous injection of CLT1-dL-(Gd-DOTA)$_4$ and sCLT1-dL-(Gd-DOTA)$_4$ at a dose of 0.03 mmol-Gd/kg in nu/nu athymic mice (n=4) bearing orthotopic human prostate tumor (* $p < 0.05$).

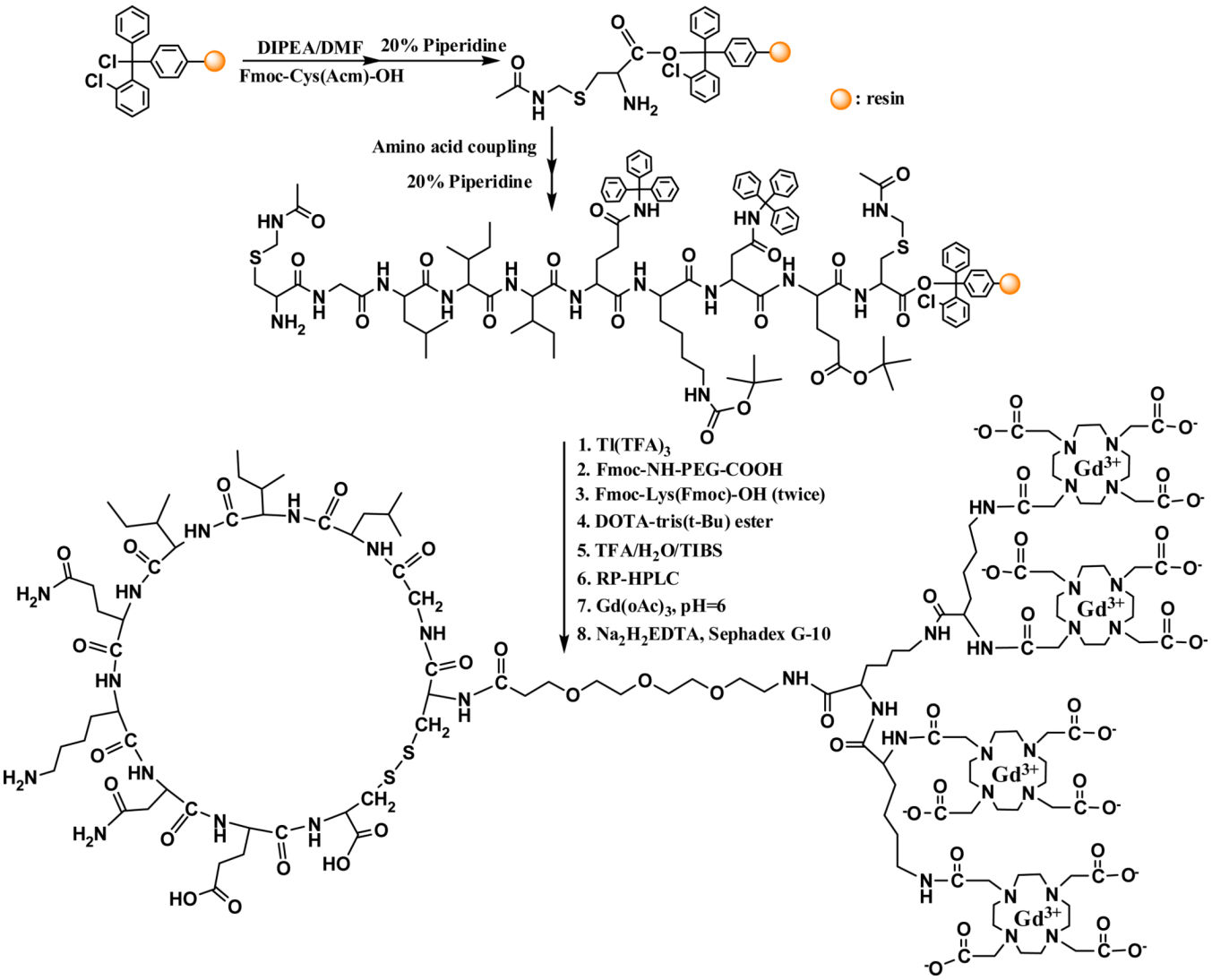

Scheme 1.
Synthesis of CLT1-dL-(Gd-DOTA)$_4$.

Table 1

Physicochemical properties of the targeted and scrambled MRI contrast agents

	r_1 ($mM^{-1}.s^{-1}$)		r_2 ($mM^{-1}.s^{-1}$)		Gd content (mmol-Gd/g)
	per Gd	**per molecule**	**per Gd**	**per molecule**	
CLT1-(Gd-DOTA)$_4$	10.1 ± 1.0	40.4 ± 3.0	13.0 ± 3.1	52.0 ± 9.6	1.05 ± 0.10
sCLT1-(Gd-DOTA)$_4$	11.5 ± 1.4	46.0 ± 5.0	12.4 ± 0.3	49.6 ± 1.3	0.97 ± 0.08
Gd-DOTA	2.9*	2.9*	3.2*	3.2*	-

*Relaxivities for Gd-DOTA in water at 37 °C are from reference 48.